

PAPER

Backscattered EM-wave manipulation using low cost 1-bit reflective surface at W-band

To cite this article: Mustafa K Taher Al-Nuaimi *et al* 2018 *J. Phys. D: Appl. Phys.* **51** 145105

View the [article online](#) for updates and enhancements.

Recent citations

- [Ultra wide band radar cross section reduction using multilayer artificial magnetic conductor metasurface](#)
Edris Ameri *et al*



IOP | ebooks™

Bringing you innovative digital publishing with leading voices to create your essential collection of books in STEM research.

Start exploring the collection - download the first chapter of every title for free.

Backscattered EM-wave manipulation using low cost 1-bit reflective surface at W-band

Mustafa K Taher Al-Nuaimi^{1,2} , Wei Hong¹ and Yejun He²

¹ State Key Laboratory of Millimeter waves, School of Information Science and Engineering, Southeast University, Nanjing 210096, People's Republic of China

² Guangdong Engineering Research Center of Base Station Antennas and Propagation, Shenzhen Key Laboratory of Antennas and Propagation, College of Information Engineering, Shenzhen University, Shenzhen 518060, People's Republic of China

E-mail: mustafa.engineer@yahoo.com

Received 17 November 2017, revised 9 February 2018

Accepted for publication 20 February 2018

Published 15 March 2018



Abstract

The design of low cost 1-bit reflective (non-absorptive) surfaces for manipulation of backscattered EM-waves and radar cross section (RCS) reduction at W-band is presented in this article. The presented surface is designed based on the reflection phase cancellation principle. The unit cell used to compose the proposed surface has an obelus (division symbol of short wire and two disks above and below) like shape printed on a grounded dielectric material. Using this unit cell, surfaces that can efficiently manipulate the backscattered RCS pattern by using the proposed obelus-shaped unit cell (as '0' element) and its mirrored unit cell (as '1' element) in one surface with a $180^\circ \pm 35^\circ$ reflection phase difference between their reflection phases are designed. The proposed surfaces can generate various kinds of backscattered RCS patterns, such as single, three, or four lobes or even a low-level (reduced RCS) diffused reflection pattern when those two unit cells are distributed randomly across the surface aperture. For experimental characterization purposes, a $50 \times 50 \text{ mm}^2$ surface is fabricated and measured.

Keywords: reflection, scattering, metasurface, EM wave

(Some figures may appear in colour only in the online journal)

1. Introduction

Manipulation of electromagnetic waves using advanced functional surfaces (also called engineered surfaces) has received considerable attention in the last decade [1, 2]. Some of the applications of those advanced functional surfaces include, for instance, anomalous reflection/refraction [3], radar cross section reduction (RCS) [4, 5], surface plasmon polariton couplers [6], cloaking [7] and polarization conversion (or rotation) [8].

Electromagnetic waves manipulation (and RCS reduction) of the backscattered EM-waves using metasurfaces (the 2D engineered surface equivalence of metamaterials) has received considerable interest recently [9–12] due to its extraordinary capability to manipulate EM waves in a very efficient manner. Manipulation of EM-waves based on coding, digital and programmable metasurface was proposed recently in [13–29].

Coding a metasurface (in its 1-bit form) requires two unit cells of 0 and π reflection phases; in other words, there is about $180 \pm 37^\circ$ phase difference between their reflection phases. In [14], a 1-bit coding metasurface was proposed for the manipulation of the backscattered EM-waves and RCS reduction around 10 GHz (7.8 GHz–12 GHz) by carefully coding ('0' or '1') the unit cells across the 1-bit metasurface aperture using a unit cell of subwavelength size ($a = 5 \text{ mm} \approx 0.166 \lambda_{10 \text{ GHz}}$). In [15], planar metasurfaces of 1-bit coding, 2-bit coding, and multi-bit coding for the manipulation and diffusion of THz waves were proposed using self-similar Minkowski closed loop like metallic resonators and the optimum distribution of the unit cells across the metasurface aperture was achieved using a particle swarm optimization algorithm. In [16], anomalous reflection (diffusion) at THz band using a conformal coding metasurface was proposed based on two unit cells formed with/without a gold ring resonator on top

of a polyimide dielectric substrate grounded by a gold film layer. In [9], a 3-bit coding reflective surface was proposed for RCS reduction around 14 GHz using a unit cell composed of a symmetric split ring and a cut wire to realize the 3-bit coding. In [10], an RCS reducer surface based on cross polarization conversion was proposed with nearly 100% polarization conversion efficiency from about 9.4 GHz–19.2 GHz. In [12], a 1-bit coding metasurface for RCS reduction was presented and the distribution of the unit cells which has three resonance frequencies was optimized using a genetic algorithm to achieve the best RCS reduction results. In [18], a flexible, non-directional 1-bit coding metasurface RCS reduction within a terahertz (THz) frequency band using square metallic ring resonators was distributed across the RCS reducer surface aperture. Recently, high optical transparency coding metasurface utilizing a flexible indium-tin-oxide (ITO)-based substrate was proposed in [22] for RCS reduction from about 8–15 GHz.

In this article, the design of a 1-bit millimeter wave (W-band) reflective (non-absorptive) surface for EM-wave manipulation and RCS reduction is presented. The proposed surface is composed by an array of unit cells of obelus (short wire and two disks above and below) like shaped resonators, patterned on one side of a dielectric substrate with a solid PEC ground on the other side. A 1-bit RCS reducer surface of random distribution of the obelus-like unit cell (as ‘0’ element) and its mirrored unit cell (as ‘1’ element), and can efficiently diffuse back the incident EM waves, is also presented based on the proposed unit cell, as will be shown in the next sections.

2. Unit cell design

The design of the presented surface begins with the design (characterization) of the unit cell used. The proposed surface is composed of an array of obelus-like shaped metallic resonators backed by a solid (continuous) metal ground plane and separated by a dielectric substrate ($\epsilon_r = 10.2$ and $h = 1.27$ mm) [30], as shown in figure 1(a). In order to assess the reflection characteristics of this unit cell, a series of full-wave numerical simulations are performed using the Frequency-Solver (based on the finite element method) of the commercial software package CST Microwave Studio [31], where the unit cell is placed in the xy -plane (around the origin point) and surrounded by a periodic boundary conditions in the x and y directions with open boundary conditions used along the $\pm z$ direction. The normally incident EM wave is then excited using a Floquet port. For the sake of completeness and clarity of the analysis, a pair of normal symmetric axes named the v -axis and u -axis are introduced along the $\pm 45^\circ$ directions, relative to the x - and y -axes, as shown in figure 1(b). Using the aforementioned simulation setup in CST Microwave Studio, the magnitude and phase of the reflected waves under the normal incidence of v -polarized and u -polarized EM-waves are computed and the results are presented in figures 1(c) and (d). As can be seen in figure 1(c), a high reflection magnitude is achieved for the waves reflected from both the v -axis and

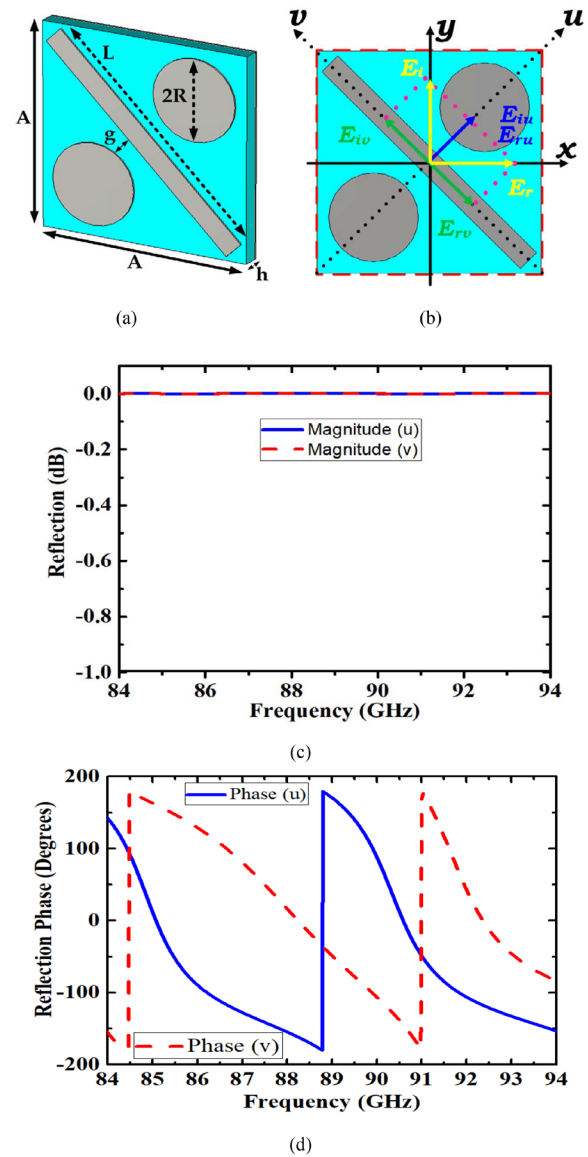


Figure 1. (a) Layout of the proposed unit cell: $L = 2.3$ mm, $A = 2$ mm, $g = 0.2$ mm, $R = 0.35$ mm, copper thickness = 0.016 mm, $\epsilon_r = 10.2$ and thickness $h = 1.27$ mm. (b) Polarization of the incident and reflected waves. Reflection (c) magnitude and (d) phase of the proposed unit cell.

u -axis with reflection phase changes between $\pm 180^\circ$ versus frequency, and there is a clear phase difference as a result of the anisotropy of the unit cell. The calculated phase difference between the reflected waves from the diagonal axes (v -axis and u -axis) is presented in figure 2. As can be seen, a phase difference of about $180^\circ \pm 35^\circ$ is achieved from about 85 GHz to 92 GHz. To further understand the reflection characteristics of the proposed unit cell, the unit cell is simulated under an x -polarized (and y -polarized) EM-wave and the results are presented in figure 3. In this article, the reflectance under the x - and y -polarized EM-waves is defined as $R_{xx} = |E_{xr}|/|E_{xi}|$, $R_{yy} = |E_{yr}|/|E_{yi}|$, $R_{xy} = |E_{xr}|/|E_{yi}|$ and $R_{yx} = |E_{yr}|/|E_{xi}|$ [9, 10]. Here, the subscripts x and y denote the polarization direction of the EM waves, and the subscripts i and r represent the incident EM waves.

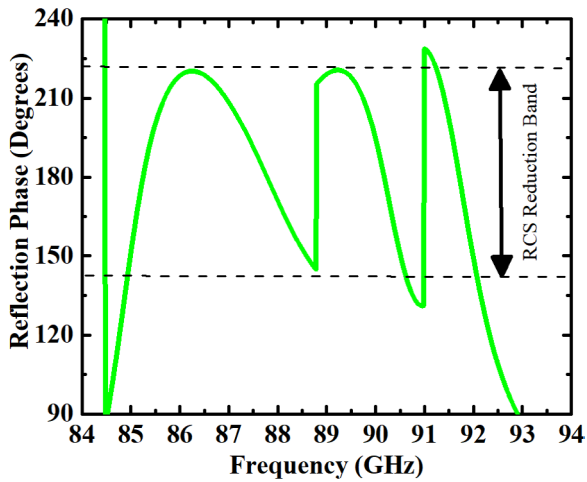


Figure 2. Reflected phase difference of the reflected waves polarized along the u -axis and v -axis.

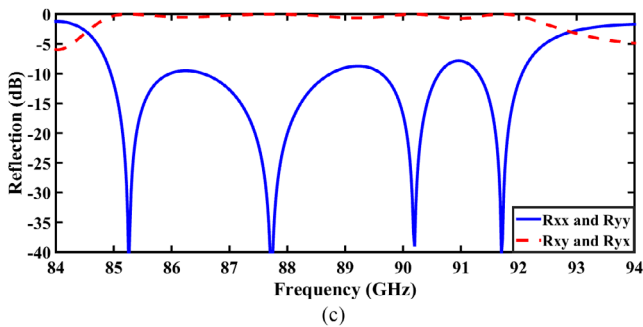


Figure 3. Reflection characteristics of the proposed unit cell under normal incidence x - and y -polarized EM-waves.

3. Reflective 1-bit surface design

The goal of this section is to investigate the capability of the unit cell proposed in the previous section to be used to design a reflective surface that can efficiently manipulate backscattered EM-waves and the backscattered RCS patterns (both shape and level) of a bare metal plate. More important is the phase difference between the reflected waves along v -axis and u -axis presented in figure 2 of the linearly polarized incident EM waves along those axes. The calculated phase difference between the reflected waves from the diagonal axes shows that a phase difference of about $180^\circ \pm 35^\circ$ is achieved from about 85 GHz to 92 GHz.

To design a 1-bit coding reflective surface as shown in [14] and to realize a $180^\circ \pm 35^\circ$ reflection phase difference between the waves reflected from the adjacent unit cells, obelus-like shape unit cell ('0' element) and its mirrored unit cell ('1' element) as shown in figure 4 are used together to compose the RCS reducer surface. Assuming that the x - or y -polarized EM-waves are impinging on the surface. Then this x - or y -polarized EM-wave would be broken into two components (E_{iu} and E_{iv}) along the u -axis and v -axis with 90° between them. However, because of the anisotropy of the unit cells, the reflected components (E_{ru} and E_{rv}) will experience a $180^\circ \pm 35^\circ$ of phase difference between them and, to realize a reflection phase cancellation across the 1-bit aperture surface,

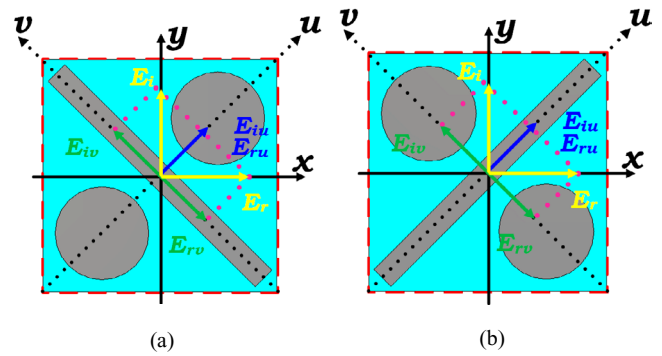


Figure 4. Front view of the (a) '0' element and (b) '1' element rotated with an angle of $\pm 45^\circ$ with respect to the x - or y -axes.

both the '0' element and '1' element can be distributed across the surface aperture in a certain manner. The cancellation of the reflected waves, in other words, the RCS reduction, and the manipulation of the backscattered power, are highly dependent on the arrangement of the unit cells across the RCS reducer surface aperture.

To validate this hypothesis, four 1-bit surfaces of unit cell distribution shown in figures 5 and 6 are designed and named as: Surface #1, Surface #2, Surface #3 and Surface #4, respectively. The presented 1-bit surfaces have an overall aperture size of $16 \times 16 \text{ mm}^2$ (8×8 unit cells). Its important here to mention that in contrast to the other three presented designs, Surface #4 has a random distribution of the '0' element and '1' element unit cells across its aperture and can be considered as a 1-bit RCS reducer surface [14, 15]. The goal of this random distribution of unit cells is to further diffuse the backscattered energy into many directions in the half space in front of the 1-bit surface. The four presented RCS reducer surfaces in figures 5 and 6 are simulated using T-solver of the commercial software CST Microwave Studio [21], where the proposed surface is placed in the xy -plane (around the origin point) and surrounded by open boundary conditions in all directions. The plane wave excitation source is used to simulate an incident wave from a source located at a large distance from the proposed surface. In combination with far-field monitors, the RCS of the surfaces is calculated.

The computed RCS 3D patterns under normal incidence are presented in figures 5 and 6 and they show that the presented designs can efficiently control the shape of the backscattered patterns. For instance, based on the unit cell distribution across the surface aperture, various backscattered patterns can be obtained, such as single beam, three beams, four beams and diffused reflection using Surface #1, Surface #2, Surface #3 and Surface #4, respectively. Compared to the classical case in which the incident and reflected angles of EM-waves are equal according to Snell's law of reflection, the presented designs can efficiently manipulate the shape of the backscattered energy with un-equal incidence and reflection angles. More important is the backscattered diffused pattern of Surface #4 in which there is no dominated lobe and incident EM-waves are redistributed on many low-level lobes in the half-space in front of the surface as a result of the destructive interference (and phase cancellation), which leads to a considerable RCS reduction.

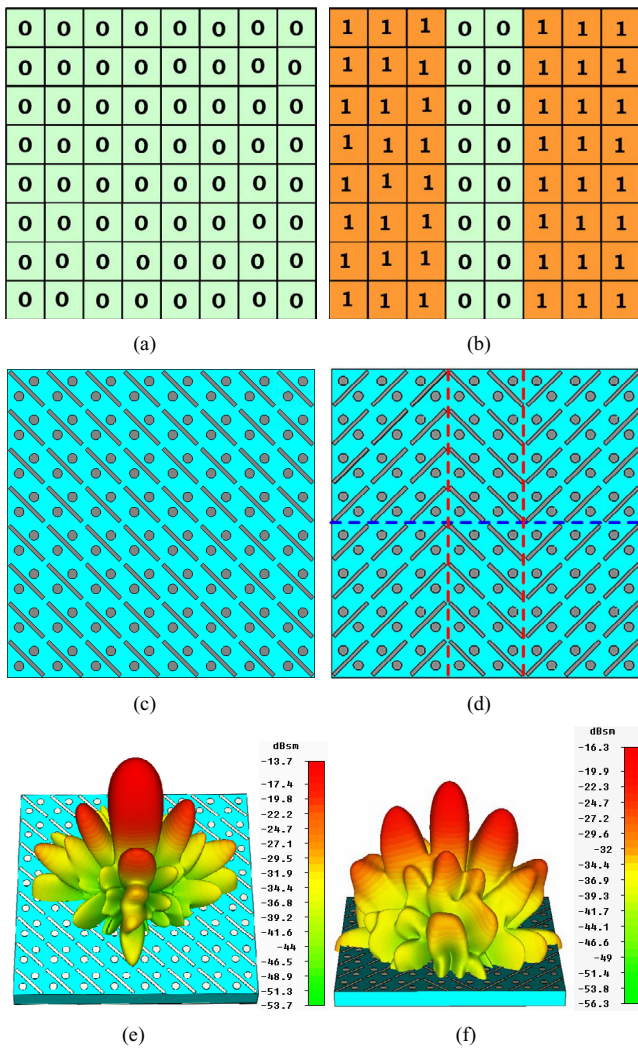


Figure 5. Unit cell distribution map of (a) Surface #1 and (b) Surface #2. Layout of (c) Surface #1, (d) Surface #2 RCS reducer surfaces and their RCS 3D patterns in (e) and (f).

To greater understand the backscattered characteristics of the presented RCS reducer surfaces, the far-field RCS rectangular patterns in different planes ($\phi = 0^\circ$, $\phi = 45^\circ$, and $\phi = 90^\circ$ planes) under normal incidence are presented in figure 7 for Surface #4. For comparison purposes, identical simulations were conducted with a bare PEC plate of equivalent geometry to that of the presented designs. In the case of Surface #4 of random distribution of unit cells across its aperture, as can be seen in figure 7, the backscattered energy is reduced in all directions (all planes), not only in the boresight direction, and the incident energy is re-distributed on many low-level minor lobes in the half space in front of the surface. The monostatic RCS versus the frequency of Surface #3 and Surface #4, along with their equivalent PEC sheet, are computed using the CST Microwave Studio and the results are presented in figure 8. RCS reduction of more than 6 dBsm is achieved from about 85 GHz to 92.2 GHz. The 2D E-field distribution of the back reflected energy in front of a bare PEC plate and Surface #4 is presented in figure 9, which shows that, for a bare PEC case, the reflected energy is a single lobe of high level along the boresight direction for all phi angles.

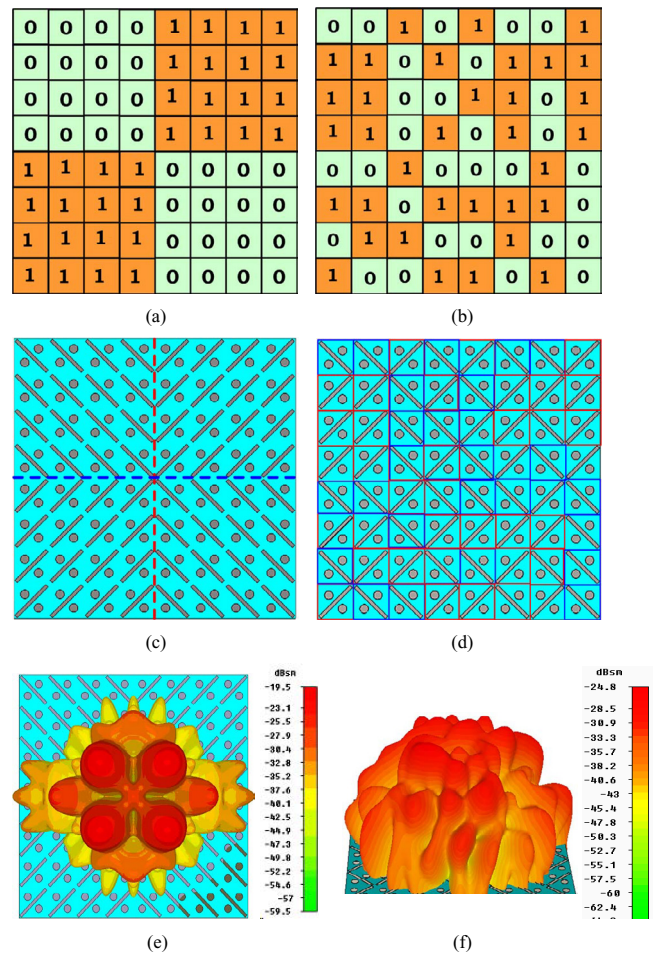


Figure 6. Unit cell distribution map of (a) Surface #3 and (b) Surface #4. Layout of (c) Surface #3, (d) Surface #4 RCS reducer surfaces and their RCS 3D patterns in (e) and (f).

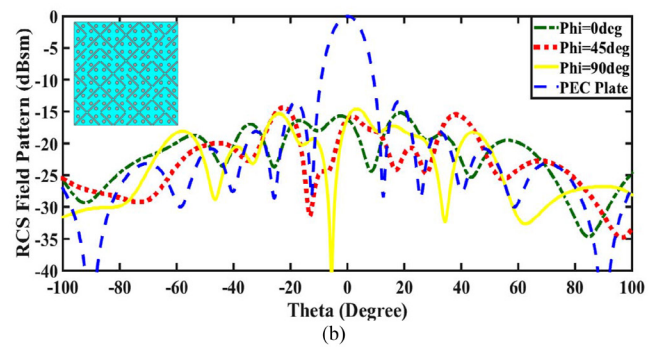


Figure 7. Backscattered RCS patterns of Surface #4 and its equivalent PEC plate.

On the other hand, and as can be seen in figure 9(b), the reflected energy is distributed on the half space in front of Surface #4 as many low-level lobes. Furthermore, the ability of Surface #4 (random distribution surface) to manipulate the backscattered RCS pattern under oblique incidence of EM-waves is investigated as well. Here, two cases are considered when $\theta_{inc} = 10^\circ$ and 45° and the backscattered RCS characteristics of Surface #4 and its equivalent bare PEC plate are investigated; the results are presented in figure 10. As can be seen in figures 10(a) and (b) for a bare PEC plate, the incident

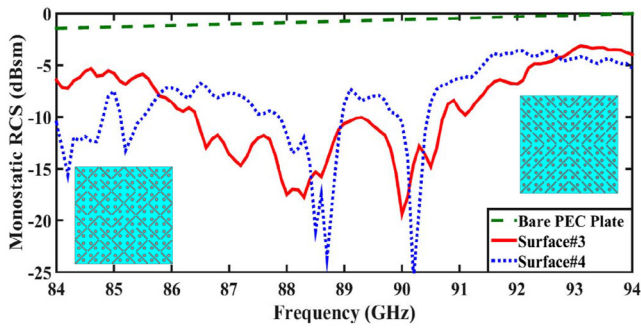


Figure 8. Monostatic RCS versus frequency plot.

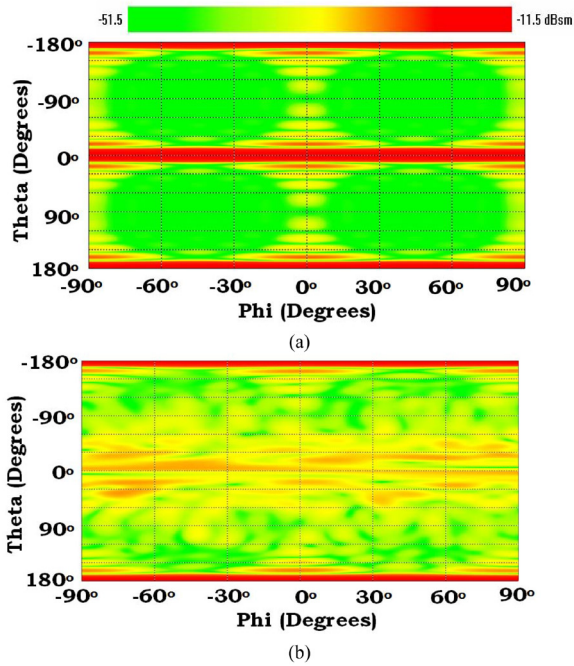


Figure 9. Backscattered 2D RCS plots of (a) bare PEC plate and (b) Surface #4.

EM-waves are reflected as high level lobes in a very predictable manner, exactly as stated by the general law of reflection (Snell’s Law) with $\theta_{inc} = \theta_{reflection}$. On the other hand, and for Surface #4 under the same angle of incidence, the backscattered RCS pattern has a diffuse reflection pattern shape of many low level lobes in all directions in the half space in front of Surface #4.

4. Fabrication and measurement results

To further verify the presented design, a sample surface is fabricated using PCB technology. The fabricated sample consists of 25×25 unit cells (aperture area of $50 \times 50 \text{ mm}^2$), as shown in figure 11, and etched on a RT/duroid 6010 high frequency laminate ($\epsilon_r = 10.2$, $h = 1.27 \text{ mm}$) [30]. The measurements are performed inside an anechoic chamber using the measurement setup shown in figure 12(a). The sample under test is placed inside a foam material, and then it is (the sample and the foam) fixed inside and surrounded by absorbers to reduce the reflections from the unwanted surroundings. Two

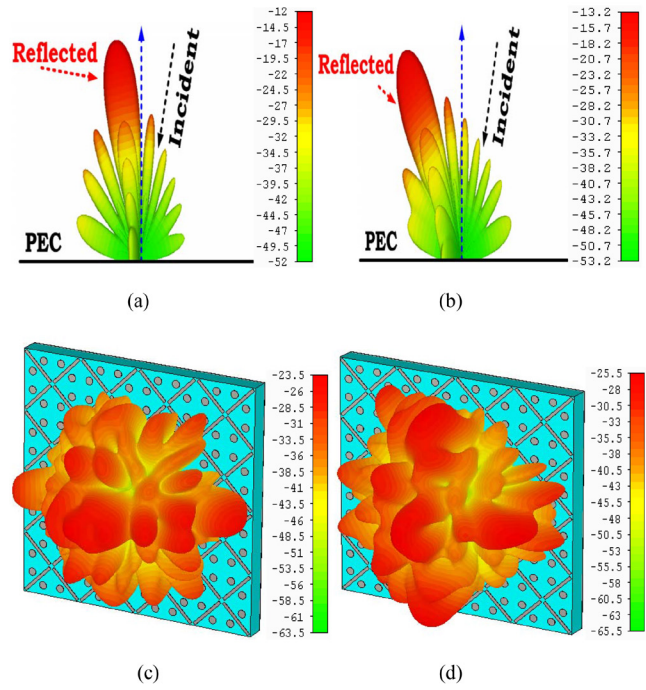


Figure 10. Backscattered RCS 3D patterns under oblique incidence of EM-waves in dBsm. PEC plate: (a) $\theta_{inc} = 10^\circ$ and (b) $\theta_{inc} = 45^\circ$. Surface #4: (c) $\theta_{inc} = 10^\circ$ and (d) $\theta_{inc} = 45^\circ$. All surfaces are placed in the xy -plane.

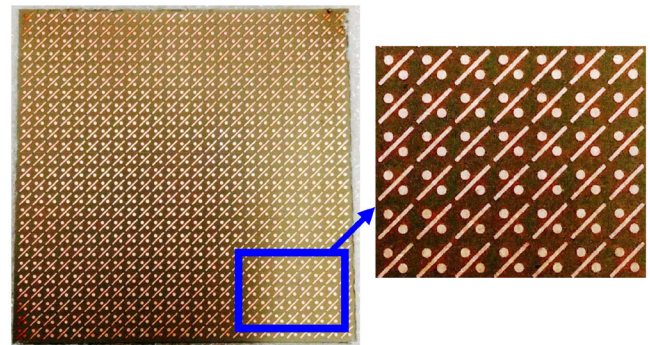


Figure 11. Photograph of the fabricated cross-polarization conversion surface.

linearly polarized rectangular horn antennas are fabricated using a 1 mm thick copper material and used as the emitter and receiver as shown in figure 12(b) along with waveguide transition parts used. The two horn antennas, serving as the transmitter and receiver, are connected (via millimeter wave extenders and flexible cables) to an Agilent N5245A network analyser, which is calibrated using Agilent V11644A mechanical cal-kit. The millimeter wave extender modules allow for extending the frequency range of the Agilent N5245A network analyzer up to 75–100 GHz [32, 33]. The horn antennas are placed adjacently (with slices of absorbers between them to reduce the mutual coupling) as high as the fabricated sample in the experiment with enough distance (R) between the horn antennas and the surface under test to avoid the near field effect. The distance R is calculated using a very well-known far-field region formula $R > (2D^2/\lambda)$ in [34], where D is the surface aperture size and λ is the free space wavelength.

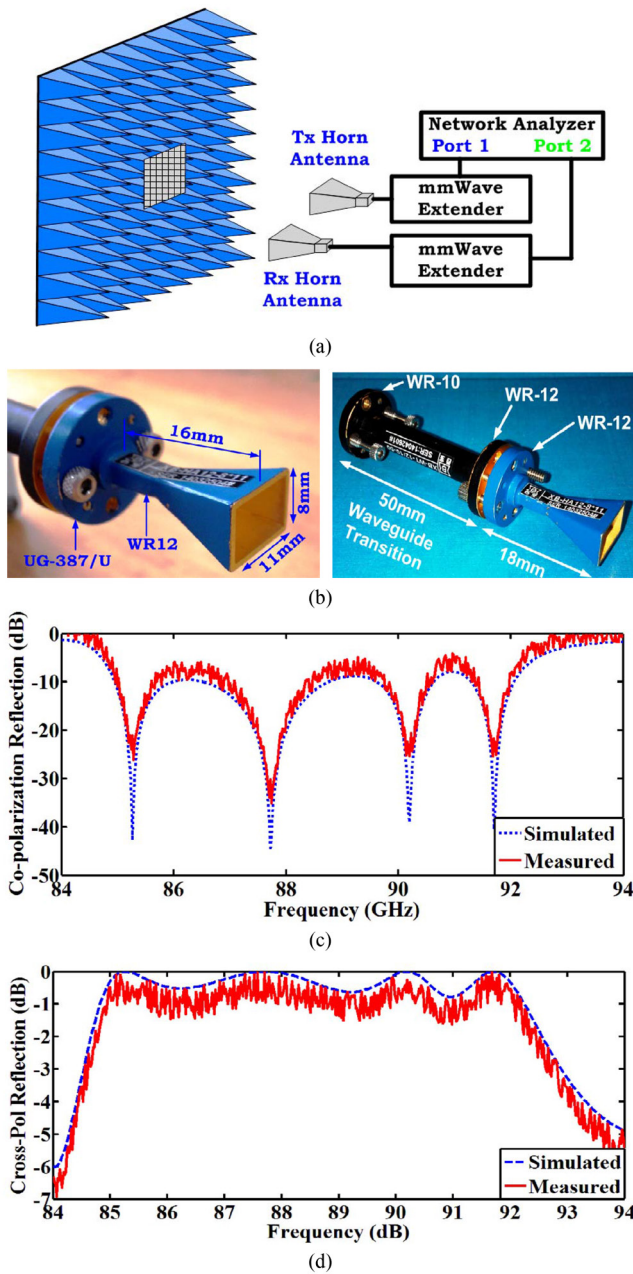


Figure 12. (a) The schematic of the measurement setup used. (b) The horn antenna used in the measurements. (c) The measured co-polarized and (d) cross-polarized reflectances.

Because of the small aperture size of the surface under test and to get more accurate measured results with low-ripple, both the IF bandwidth and the output power have been chosen carefully [22, 23].

The measured co-pol and cross-pol reflected waves are presented in figures 12(c) and (d) for frequencies from 84 GHz to 94 GHz. The small acceptable discrepancies between the measured and simulated results in figure 3 can be attributed to (i) fabrication inaccuracies of the surface, (ii) the misalignments between the antennas and the surface under test during the measurements, where, with the help of a laser pointer, a manual alignment is performed [22, 23], (iii) in the simulation, the proposed surface is excited with a far-field plane wave, which is not the case in the measurements where a couple

of horn antennas are used instead, (iv) in the simulation, the plane wave is normally incident on the proposed surface, which is not the case in measurements where the antennas had to be tilted with a certain angle and the plane wave will not hit the surface with an exactly normal angle.

5. Conclusion


In this article, the design of low cost reflective surface for EM-wave manipulation and RS reduction for 84 GHz to 94 GHz band is presented and investigated both numerically and experimentally. The presented design can efficiently manipulate the shape and level of the backscattered EM waves and various backscattered patterns ranging from a single beam, three beams and four beams, and diffuse reflection is achieved.

Acknowledgments

The authors would like to thank the anonymous reviewers for their helpful and constructive comments that greatly contributed to improving the quality of the final version of the article. They would also like to thank the Editors for their generous comments and support during the review process. The authors would like to thank Professor Z Q Kuai and Mr H T Yi for the help with fabrication of the horn antennas and the presented surfaces.

The third author would like to thank the National Natural Science Foundation of China for in part supporting this work under Grant 61372077, in part by the Shenzhen Science and Technology Programs under Grant ZDSYS 201507031550105, JCYJ20170302150411789, JCYJ20170 302142515949 and GCZX2017040715180580, as well as in part by the Guangdong Provincial Science and Technology Program under Grant 2016B090918080.

ORCID iDs

Mustafa K Taher Al-Nuaimi  <https://orcid.org/0000-0001-7876-616X>

References

- [1] Yu N F and Capasso F 2014 Flat optics with designer metasurfaces *Nat. Mater.* **13** 139
- [2] Yu N F *et al* 2011 Light propagation with phase discontinuities: generalized laws of reflection and refraction *Science* **334** 333–7
- [3] Li H, Wang G, Xu H, Cai T and Liang J 2015 X-band phase-gradient metasurface for high-gain lens antenna application *IEEE Trans. Antennas Propag.* **63** 5144–9
- [4] Chen W, Balanis C A and Birtcher C 2015 Checkerboard EBG surfaces for wideband radar cross section reduction *IEEE Trans. Antennas Propag.* **63** 2636–45
- [5] Galarregui J C I *et al* 2013 Broadband radar cross-section reduction using AMC technology *IEEE Trans. Antennas Propag.* **61** 6136–43
- [6] Sun S L, He Q, Xiao S Y, Xu Q, Li X and Zhou L 2012 Gradient-index meta-surfaces as a bridge linking propagating waves and surface waves *Nat. Mater.* **11** 426

- [7] Alù A and Engheta N 2008 Plasmonic and metamaterial cloaking: physical mechanisms and potentials *J. Opt. A: Pure Appl. Opt.* **10** 2008
- [8] Liu X, Zhang J, Wei L, Lu R, Li L, Xu Z and Zhang A 2016 Three-band polarization converter based on reflective metasurface *IEEE Antennas Wirel. Propag. Lett.* **16** 924–7
- [9] Su P, Zhao Y, Jia S, Shi W and Wang H 2015 An ultra-wideband and polarization-independent metasurface for RCS reduction *Sci. Rep.* **6** 20387
- [10] Jiang W, Xue Y and Gong S 2016 Polarization conversion metasurface for broadband radar cross section reduction *Prog. Electromagn. Res. Lett.* **62** 9–15
- [11] Jia Y, Liu Y, Guo Y J, Li K and Gong S X 2016 Broadband polarization rotation reflective surfaces and their applications to RCS reduction *IEEE Trans. Antennas Propag.* **64** 179–88
- [12] Sun H et al 2017 Broadband and broad-angle polarization-independent metasurface for radar cross section reduction *Sci. Rep.* **7** 40782
- [13] Giovampaola C D and Engheta N 2014 Digital metamaterials *Nat. Mater.* **13** 1115–21
- [14] Cui T J, Qi M Q, Wan X, Zhao J and Cheng Q 2014 Coding metamaterials, digital metamaterials and programmable metamaterials *Light Sci. Appl.* **3** e218
- [15] Gao L-H et al 2015 Broadband diffusion of terahertz waves by multi-bit coding metasurfaces *Light Sci. Appl.* **4** e324
- [16] Liang L J et al 2015 Anomalous terahertz reflection and scattering by flexible and conformal coding metamaterials *Adv. Opt. Mater.* **3** 1374–80
- [17] Liu S et al 2015 Polarization-controlled anisotropic coding metamaterials at terahertz frequencies (arXiv:1509.03692)
- [18] Xin Y, Lan-Ju L, Ya-Ting Z, Xin D and Jian-Quan Y 2015 A coding metasurfaces used for wideband radar cross section reduction in terahertz frequencies *Acta Phys. Sin.* **64** 158101
- [19] Yan X et al 2015 Broadband, wide-angle, low-scattering terahertz wave by a flexible 2-bit coding metasurface *Opt. Express* **23** 29128–37
- [20] Zhuang Y, Wang G, Liang J, Cai T, Tang X, Guo T and Zhang Q 2017 Random combinatorial gradient metasurface for broadband, wide-angle and polarization-independent diffusion scattering *Sci. Rep.* **7** 16560
- [21] Sui S, Ma H, Wang J, Pang Y, Feng M, Xu Z and Su Q 2017 Absorptive coding metasurface for further radar cross section reduction *J. Phys. D: Appl. Phys.* **51** 065603
- [22] Chen K, Cui L, Feng Y, Zhao J, Jiang T and Zhu B 2017 Coding metasurface for broadband microwave scattering reduction with optical transparency *Opt. Express* **25** 5571–9
- [23] Zhuang Y, Wang G and Xu H 2017 Ultra-wideband RCS reduction using novel configured chessboard metasurface *Chin. Phys. B* **26** 054101
- [24] Cui L, Wang W, Ding G, Chen K, Zhao J, Jiang T, Zhu B and Feng Y 2017 Polarization-dependent bi-functional metasurface for directive radiation and diffusion-like scattering *AIP Adv.* **7** 115214
- [25] Xu H X, Ma S, Ling X, Zhang X-K, Tang S, Cai T, Sun S L, He Q and Zhou L 2017 Deterministic approach to achieve broadband polarization-independent diffusive scatterings based on metasurfaces *ACS Photon.* (<https://doi.org/10.1021/acsp Photonics.7b01036>) accepted
- [26] Zheng Y, Zhou Y, Gao J, Cao X, Yang H, Li S, Xu L, Lan J and Jidi L 2017 Ultra-wideband polarization conversion metasurface and its application cases for antenna radiation enhancement and scattering suppression *Sci. Rep.* **7** 16137
- [27] Yuan F, Wang G, Xu H, Cai T, Zou X and Pang Z 2017 Broadband RCS reduction based on spiral-coded metasurface *IEEE Antennas Wirel. Propag. Lett.* **16** 3188–91
- [28] Cui T, Liu S and Zhang L 2017 Information metamaterials and metasurfaces *J. Mater. Chem. C* **5** 3644–68
- [29] Liu X, Gao J, Xu L, Cao X, Zhao Y and Li S 2017 A coding diffuse metasurface for RCS reduction *IEEE Antennas Wirel. Propag. Lett.* **16** 724–7
- [30] Rogers Corporation www.rogerscorp.com
- [31] CST Microwave Studio 3D EM Simulation Software www.cst.com/products/cstmws
- [32] Vasanelli C, Boegelsack F and Waldschmidt C 2016 Design and experimental characterization of a surface with low radar cross-section at millimeter-wave frequencies 2016 46th European Microwave Conf. (EuMC) (London) pp 21–4
- [33] Alvarez Y, de Cos M E and Las-Heras F 2010 RCS measurement setup for periodic-structure prototype characterization *IEEE Antennas Propag. Mag.* **52** 100–6
- [34] Balanis C A 1996 *Antenna Theory, Analysis and Design* 2nd edn (New York: Wiley)